Bull. Mater. Sci., Vol. 26, No. 1, January 2003, pp. 79–89. © Indian Academy of Sciences.

A first-principles thermodynamic approach to ordering in binary alloys

ABHIJIT MOOKERJEE*, TANUSRI SAHA-DASGUPTA, I DASGUPTA, A ARYA[†], S BANERJEE[†] and G P DAS[#]**

S.N. Bose National Centre for Basic Sciences, JD-Block, Sector III, Salt Lake, Kolkata 700 098, India
**Department of Physics, Indian Institute of Technology, Powai, Mumbai 400 076, India
[†]Materials Science Division, [#]TP&PE Division, Bhabha Atomic Research Centre, Mumbai 400 085, India

Abstract. The communication reviews the augmented space based approaches to thermodynamics and ordering of binary alloys. We give several examples of metallic alloys to illustrate our methodology.

Keywords. Phase stability; binary alloys; phase segregation.

1. Introduction

During the last decade, immense strides in the development of first principles electronic structure and total energy techniques have brought computational physicists in close contact with metallurgists. The feasibility of near-quantitative, predictive possibilities have made this contact fruitful. The practicing metallurgist makes frequent use of empirical principles or rule of the thumb. These have been gleaned from extensive physical insight gained from experiments over a large class of systems, over a long period of time. A few examples relevant to our area of interest are the Hume–Rotherý rules, which relate alloy stability to band filling, constituent size differences and charge transfer; the Phillips' rule, which states that prevalently ionic tetravalent semiconductors tend to go into the wurzite structure, while prevalently covalent ones stabilize in the diamond or ZnS structure and the Pettifor rule which bunches elements in the Mendeleév table and relates similar alloying properties to the groups. While these rules are of great value to an experimental metallurgist, there are several drawbacks. The rules are purely empirical and we do not know why they work in some circumstances and also why they sometimes fail in others. Independent parameters are often not recognized. Even if they are, the metric in parameter space is not always defined. Systems with nearby parameters often have quite different behaviour. It is, therefore, important to understand from microscopic theories why such rules work in the first place. Consequently we should be able to understand why they fail in other circumstances, so that we may modify and extend these rules to robust theories which work over a very large class of systems. The importance of first-principles theories with well-understood approximations and error estimates is also paramount. While we may like to play with parametrized theories, particularly to gain physical insight, we should not forget the adage, 'Given enough parameters you can fit your grandmother to an elephant'!

The study of alloy thermodynamics requires basically the calculation of the Gibbs free energy, i.e. the internal energy and the entropy. Let us examine these in some detail. An accurate estimate of the internal energy at low temperatures may be obtained from one of the many sophisticated, first-principles, electronic structure methods currently available with us: among others, the Korriga–Kohn–Rostocker (KKR) and its related linearized muffin–tin orbitals method (LMTO), in particular in its tight-binding incarnation (TB–LMTO) (Andersen 1975; Andersen and Jepsen 1984; Andersen *et al* 1991); the augmented plane wave (APW) and its linearized version (LAPW) and the pseudopotential based methods. Such methods have been developed for crystalline materials as well as disordered systems, in conjunction with mean-field approaches like the coherent potential approximation (CPA) and the augmented space method based techniques: augmented space recursion (ASR) (Mookerjee 1973; Kumar *et al* 1982; Saha *et al* 1994; Dasgupta *et al* 1995; Saha and Mookerjee 1997) and the travelling cluster approximation (TCA) (Kaplan and Gray 1976; Kaplan *et al* 1980), both of which take into account configuration fluctuations. The recursion method also allows us to deal with extended impurities, dislocations and rough interfaces. Entropy estimation is a more difficult task. The cluster variation method is available to us. Phonon contribution to the entropy is important in many circumstances.

The concentration wave approach of Khatchaturyan (1978, 1983) starts from a completely disordered phase and sets it up in a concentration wave appropriate to the ordering to be studied. It then studies where in the tem-

*Author for correspondence

perature-concentration phase plane the disordered phase becomes unstable to the perturbation. In the completely disordered phase each site, R, has an occupation variable, n_R, associated with it. For homogeneous perfect disorder we have $\langle\langle n_R\rangle\rangle = x$, where x is the concentration of one of the components of the alloy. In this homogeneously disordered system, we introduce fluctuations in n_R at each site: $\delta x_R = n_R - x$. We expand the energy of this new configuration with concentration fluctuations at each site as

$$E(C) = E^{(0)} + \sum_{R}^{N} E_R^{(1)} \delta x_R + \sum_{RR'}^{N} E_{RR'}^{(2)} \delta x_R \delta x_{R'} + \ldots \qquad (1)$$

The coefficients $E^{(0)}$, $E_R^{(1)}$ … are the effective renormalized cluster interactions (EPIs) in which the contributions from self-retraced paths have been included. $E^{(0)}$ is the energy of the averaged disordered medium. If we embed atoms of the type A or B in the homogeneously disordered medium at the site, R, it follows from (1) that

$$E_R^{(1)} = E_R^{(A)} - E_R^{(B)}.$$

$E_R^{(1)}$ is a single body interaction resulting from the interchange of a B atom with an A atom at site R in the alloy. Similarly, $E_{RR'}^{(2)}$ is the effective renormalized pair interaction which is the difference in the single body interaction at R, when sites $R'(\neq R)$ is occupied either by A or B atom

$$E_{RR'}^{(2)} = E_{RR'}^{(AA)} + E_{RR'}^{(BB)} - E_{RR'}^{(AB)} - E_{RR'}^{(BA)}.$$

The renormalized pair interactions are the correlations between two sites and are the dominant quantities for the analysis of phase stability. We shall use the symbol, V_n, for $E_{RR'}^{(2)}$, where $R - R' = \gamma_n$, the nth nearest neighbour vector on the underlying lattice. We usually retain terms up to pair interactions in the configuration energy expansion. Higher order interactions may be included for a more accurate and complete description. They are essential for many structural transitions between complex phases involving large unit cells.

The effective pair interactions can be related to the change in the configuration averaged local density of states

$$V_n = \int_{-\infty}^{E_F} \mathrm{d}E (E - E_F) \Delta n(E),$$

where $\Delta n(E)$ is given by

$$\Delta n(E) = \sum_{IJ \in \text{all pairs}} \Im m \langle\langle \mathrm{Tr}(EI - H^{(IJ)})^{-1} \rangle\rangle \chi_{IJ}.$$

χ_{IJ} is ± 1 according to whether $I = J$ or $I \neq J$. There are four possible pairs at IJ: AA, AB, BA and BB. H^{IJ} is the Hamiltonian of a system where all sites except R and R' are randomly occupied. The sites R and R' are occupied by atoms of the types I and J. This change in the averaged local density of states can be related to the generalized phase shift, $\delta(E)$, through the equation

$$\Delta n(E) = \frac{\mathrm{d}\delta(E)}{\mathrm{d}E},$$

where $\delta(E)$ is

$$\delta(E) = \log \frac{\det \langle\langle G^{AA} \rangle\rangle \det \langle\langle G^{BB} \rangle\rangle}{\det \langle\langle G^{AB} \rangle\rangle \det \langle\langle G^{BA} \rangle\rangle}.$$

G^{IJ} is the resolvent of the Hamiltonian H^{IJ}. The generalized phase shift, $\delta(E)$, can be calculated following the orbital peeling method of Burke (1976). We shall quote only the final result

$$V_n = \sum_{IJ \in \text{all pairs}} \sum_{\alpha=1}^{9} \chi_{IJ} \int_{-\infty}^{E_F} (E - E_F) \log \langle\langle G_\alpha^{IJ} \rangle\rangle$$

$$= \sum_{IJ \in \text{all pairs}} \sum_{\alpha=1}^{9} \left[\sum_{k=1}^{p-1} Z_k^{\alpha,IJ} - \sum_{k=1}^{p} P_k^{\alpha,IJ} + (N_P^{\alpha,IJ} - N_Z^{\alpha,IJ}) E_F \right]. \qquad (2)$$

$\langle\langle G_\alpha^{IJ} \rangle\rangle$ denotes the configuration averaged Green function corresponding to the Hamiltonian in which two atoms of the type I and J are embedded at sites R and R' and in which the orbitals from $L = 1$ to $(\alpha - 1)$ are deleted at the site R. $Z_k^{\alpha,JJ}$ and $P_k^{\alpha,IJ}$ are its zeros and poles and $N_Z^{\alpha,IJ}$ and $N_P^{\alpha,IJ}$ are the number of such zeros and poles below E_F. This method of zeros and poles enables one to carry out the integration easily avoiding the multivaluedness of the integrand involved in the evaluation of the integral by parts. The positions and number of zeros and poles are estimated from the recursion coefficients for $\langle\langle G_\alpha^{IJ} \rangle\rangle$.

We propose to use the function

$$V_n(E, x) = \int_{-\infty}^{E} \mathrm{d}E (E - E_F) \Delta n(E),$$

with $V_n(E_F, x) = V_n$. This sign of this function at the Fermi energy decides whether in the ground state, an alloy will form or phase segregate. This replaces the first of the Hume-Rotherý rule and gives an accurate prediction of alloying or phase segregation.

1.1 *The concentration wave analysis*

In the concentration wave model (Khatchaturyan 1978, 1983), the occupation probability, $n(R)$, at any lattice position, $R(p)$, and its Fourier transform, the concentration wave amplitude are given by

$$n(R) = \sum_{h=1}^{N} Q(\underline{k}) \exp\{-i\underline{k}(h) \cdot R(p)\};$$

$$Q(\underline{k}) = \frac{1}{N} \sum_{p=1}^{N} n(R) \exp\{i\underline{k}(h) \cdot R(p)\}.$$

The first summation is over the N lattice points of the periodic crystal and the second is over the N points of the first Brillouin zone. The wave-vector, $\underline{k}(h)$, and the lattice vector, $R(p)$, are defined by

$R(p) = p_\alpha \mathbf{a}_\alpha$ ($\alpha = 1, 2, 3$; p_α are integers, summation implied),
$\underline{k}(h) = 2\pi h_a \mathbf{b}_a$ ($h_a = m_a/N_a$, $m_a = 0, \pm 1, \pm 2, \ldots$),

where $\mathbf{a}_a$ and $\mathbf{b}_a$ are lattice translation vectors and primitive translation vectors of the reciprocal lattice such that $\mathbf{a}_a \cdot \mathbf{b}_a = \delta_{ab}$.

The concentration wave amplitude, $Q(\underline{k})$, corresponding to the wave vector, $\underline{k}$, that generates the ordering instability are expressed in terms of normalized (with respect to the concentration, x) long range order parameter, $\tilde{\eta}(\underline{k})$, via the following relation

$$Q(\underline{k}) = x \cdot \tilde{\eta}(\underline{k}).$$

The normalized order parameter, $\tilde{\eta}(\underline{k})$, is related to the standard order parameter ($\eta(\underline{k})$), as $\tilde{\eta}(\underline{k}) = \eta(\underline{k}) / \eta_{\max}(\underline{k})$, where $\eta_{\max}(\underline{k})$ is the maximum order parameter attainable at a given composition. The internal energy, in the pair approximation up to an arbitrary coordination shell, is given as

$$E = \frac{N}{2} \sum_{h=1}^{N} V(\underline{k}(h)) \cdot Q(\underline{k}(h)) Q^*(\underline{k}(h)),$$

where $Q(\underline{k})$ is the amplitude of the concentration wave and $V(\underline{k})$ the Fourier transforms of the pair interactions, are given by

$$V(\underline{k}) = 1/N \sum_{p=1}^{N} V(R) \exp\{i\underline{k}(h) \cdot R(p)\}.$$

The expression for the configurational entropy is given as

$$S = k_B \sum_{p=1}^{N} [n(R(p)) \ln(n(R(p))) + (1 - n(R(p))) \ln(1 - n(R(p)))],$$

which, in terms of sub-lattice probabilities, can be expressed as

$$S = k_B \sum_{\mathcal{S}=1}^{\mathcal{T}} N_{\mathcal{S}} [n_{\mathcal{S}} \ln n_{\mathcal{S}} + (1 - n_{\mathcal{S}}) \ln(1 - n_{\mathcal{S}})], \quad (3)$$

where $\mathcal{T}$ is the total number of sublattices, $n_{\mathcal{S}}$ and $N_{\mathcal{S}}$ are the occupation probability and the number of atoms on the $\mathcal{S}$th sub-lattice, respectively.

The effective pair interactions, $V(\underline{k})$ for the wave vector, $\underline{k}(h)$ with components (h_1, h_2, h_3), are related to those in the real space V_2(s) as

$$V(\underline{k}) = \sum_{(s)} f_{\underline{k}}^{(s)} V_s, \quad (4)$$

where, for the *fcc* and the *bcc* lattices, the shell functions, $f_{\mathbf{k}}^{(s)}$, for an arbitrary coordination shell 's' are given by the formulae (de Fontaine 1975)

$$f_k^{(s)} = \frac{z^{(s)}}{6} \sum_{j=1}^{3} \cos(2\pi h_1 p_j^{(s)}) \ldots \ldots [\cos(2\pi h_2 p_{j+1}^{(s)}) \cos(2\pi h_3 p_{j+2}^{(s)}) + \cos(2\pi h_3 p_{j+1}^{(s)}) \cos(2\pi h_2 p_{j+2}^{(s)})], \quad (5)$$

where $z^{(s)}$ is the number of lattice points in the coordination shell 's', $p_j^{(s)}$ are integers and half-integers denoting the Cartesian coordinates of a point in the first octant of the shell 's' and 'h_i' denotes the Cartesian coordinates in the first Brillouin zone.

1.2 *Study of phase segregation in PdRh*

We shall first study the alloy system, PdRh, where the constituents phase segregate as we lower the temperature. It is one of the few alloy systems which do not show polymorphism and there is relatively little charge transfer or size disparity between the constituents. The Hume–Rotherý rules predict phase segregation at low temperatures as the *d*-band filling is almost complete.

We carry out a calculation of the nearest neighbour pair energies for PdRh alloys using the TB–LMTO–ASR coupled with orbital peeling and the results are shown in figure 1.

The effective pair energy at the Fermi level is negative for all concentrations. The pair interactions in PdRh decay very rapidly with distance and the dominant interaction, V_1, is negative for all concentrations. This indicates that atoms in PdRh like to be surrounded by similar atoms. This means that at low temperatures PdRh phase segregates into domains, some enriched by Pd and others by Rh. The alloy exists as a mixture of these phases.

We have already interpreted the process of ordering or segregation in binary alloys as the loss of stability of a perfectly disordered solution with respect to static concentration wave perturbations. The minimization of free energy will be achieved when the configurational energy reaches a minimum allowable value. This configurational energy under the pair interaction approximation can be

represented in Fourier space as a product of the Fourier transform of the effective pair energies and the concentration fluctuation pair correlation function

$$E = (N/2)\sum_{\underline{k}} V(\underline{k})Q(\underline{k})Q^*(\underline{k}).$$

The minimization of E will naturally occur for states of order characterized by maxima in $|Q(\underline{k})|^2 = \langle\langle \sigma_{\underline{k}R}\sigma_{\underline{k}R'}\rangle\rangle$ located in the regions of the absolute minima of $V(\underline{k})$. Consequently we can learn a lot about the types of possible orderings from the study of the shape of $V(\underline{k})$ and search of its absolute minima. These are called the Lifshitz points. Different types of orderings are related to these special Lifshitz points. In particular, a minimum at the Γ-point indicates phase segregation, while one at the X-point in a face-centred cubic lattice indicates a $L1_0$ or $L1_2$ type or ordering at low temperatures. Peaks away from the special points indicate long period superstructures, as we shall see for NiMo alloys.

We have calculated $V(\underline{k})$ by summing up V_n with appropriate weights up to the sixth nearest neighbour shells. Figure 2 (right) shows the fast convergence of V_n with n.

The stability limit of the concentration wave, i.e. the temperature at which the disordered phase becomes unstable is determined by the vanishing of the derivative of the free energy. The ordering spinodal is defined as the region in the temperature-concentration diagram below which the disordered alloy is unstable and separates into Pd-rich and Rh-rich domains. In the region just outside the spinodal the alloy is metastable and will phase separate, given sufficient diffusion. The region of metastability continues to the phase boundary beyond which the solid solution exhibits clustering type short-ranged order, but will not segregate.

In the spirit of the Landau expansion, if we expand the configurational Gibbs free energy in terms of the concentration wave amplitude order parameter, the quadratic term is

$$F^{(2)} = (N/2)\sum_{\underline{k}} F(\underline{k})\,|\,\tilde{\eta}(\underline{k})\,|^2,$$

where $F(\underline{k}) = k_B T + V(\underline{k})x(1-x)$. At the stability point this vanishes, giving us

$$T_0 = \frac{-x(1-x)V(\underline{k})}{k_B}.$$

In case the pair energy $V(\underline{k})$ is independent of concentration, the spinodal curve will always be symmetric about $x = 0{\cdot}5$. It is the concentration dependence of $V(\underline{k})$ which gives rise to the asymmetry of the spinodal.

Figure 3 shows the spinodal for PdRh. There is asymmetry about $x = 0{\cdot}5$. We can understand this physically as follows: Pure Rh has a smaller equilibrium volume than Pd. Thus the Pd–Rh distance will be on the whole larger in the Pd-rich side of the phase diagram. This indicates that the nearest neighbour energy is more attractive on the Rh-rich side. The maximum point on the spinodal curve corresponds to the maximum temperature of the miscibility gap, comes out to be 1350°. This is 160° higher than that experimentally observed (Shield and Williams 1987). The over-estimation is a characteristic of the Bragg–Williams approximation. If we carry out the tetrahedron–octahedron approximation in the cluster variation technique and include the phononic contribution to the Gibbs free energy, we obtain the maximum spinodal

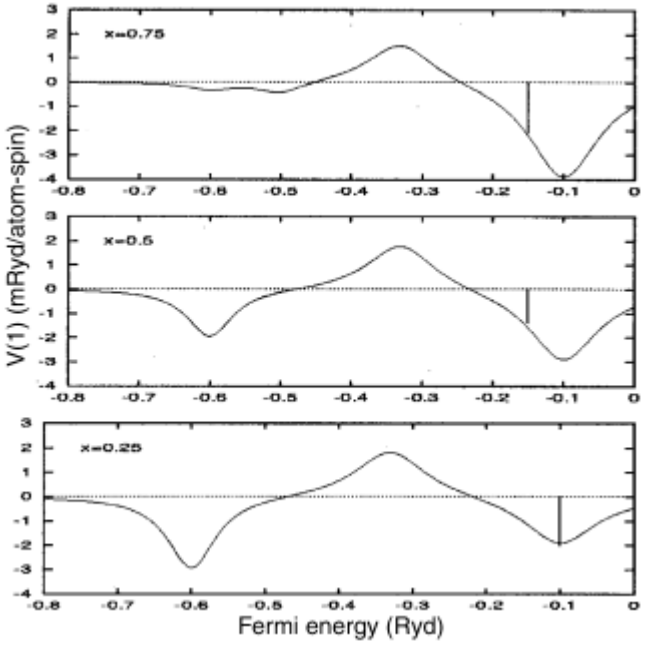

Figure 1. The variation of the nearest neighbour pair energies as a function of energy for Pd_xRh_y alloys. The Fermi energies are shown as vertical lines.

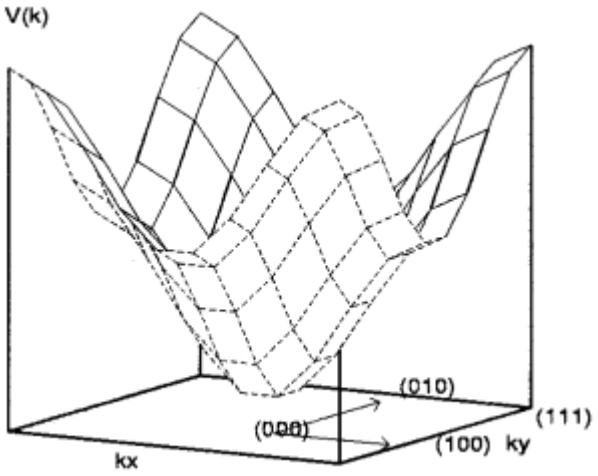

Figure 2. The surface $V(\underline{k})$ at $k_x = 0$ for 50–50 PdRh.

temperature to within 10–20° of the experimental value (Wolverston *et al* 1993). Similar agreement has been obtained by Wang *et al* (1993) using Monte Carlo techniques.

1.3 *Study of phase ordering in NiMo*[†]

The Ni-rich side of the Ni–Mo system (see figure 4) (Shunk 1969) has three equilibrium ordered inter-metallic phases viz. β-Ni_4Mo ($D1_a$), γ-Ni_3Mo (DO_a) and δ NiMo ($P2_12_12_1$).

The coherent LRO structures which are encountered in the Ni–Mo alloy system belong to the $\langle 1\frac{1}{2}0\rangle$ family. These structures viz. Ni_4Mo ($D1_a$), Ni_3Mo (DO_{22}), Ni_2Mo (Pt_2Mo type) and Ni_2Mo_2 ($I4_1/amd$) can be described (de Fontaine 1975; Khatchaturyan 1978; Kulkarni and Banerjee 1988) in terms of stacking of (420) planes (see figure 5) that contain either all Ni or all Mo atoms. These members of the (420) series are generally designated as N_4M, N_3M, N_2M and N_2M_2, respectively.

The concentration wave description (Khatchaturyan 1978) of these superstructures is described by the concentration delta function, $C(p)$, written as a function of the magnitude of the vector $\underline{p}$ in terms of the plane indices $\underline{p} = p\langle lmn\rangle$. $C(p)$ is equal to unity at the plane, $p = 0$ and zero elsewhere ($p = 1, \ldots, N-1$), so that the concentration Fourier spectrum along a specific vector $\underline{k}$ is given by

$$C(\underline{k}) = \frac{1}{N}\sum_{p=0}^{N-1} C(p)\exp(-2\pi i\underline{k}\cdot\underline{p}). \tag{6}$$

For each structure, there are exactly $N(= 2, 3, 4, 5)$ Fourier waves of same amplitude.

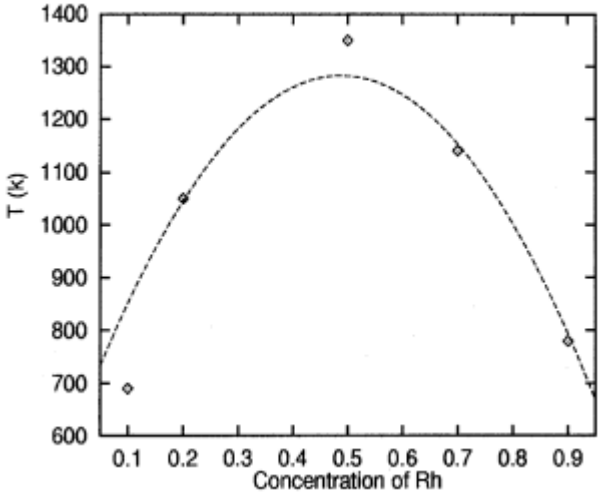

Figure 3. The spinodal curve for PdRh.

[†]Contents of this section has been discussed in an earlier paper also (Arya *et al* 2001)

1.3a *Concentration wave description of the superstructures:* We shall first describe the concentration waves that lead to the structures relevant to the NiMo system.

Ni_4Mo ($D1_a$) structure

The unit cell of Ni_4Mo structure can be described as a layered structure of (420) layers with every fifth layer being occupied entirely by Mo atoms while the intervening four layers being filled by Ni atoms. The wave representation of such a structure or the occupation probability of Mo atoms on the pth (420) layer can be expressed as (see figure 5)

$$C(p) = x + \frac{2}{5}\eta\left(\cos\frac{2\pi p}{5} + \cos\frac{4\pi p}{5}\right). \tag{7}$$

For stoichiometric composition, ($x_{Mo}\equiv$) $x = \frac{1}{5}$, and for order parameter, $\eta = 1$ (i.e. fully ordered), the (420) layered structure of Ni_4Mo will, therefore, be, 'Mo Ni Ni Ni Ni Mo…'. This structure can be viewed as a super-imposition of $\frac{i}{5}\langle 420\rangle$ (i = 1 to 4) waves.

Ni_3Mo (DO_{22}) structure

The concentration wave description of the DO_{22} structure (which also may be described as a (420) layered structure) is given by (figure 5)

$$C(p) = x + \frac{1}{4}\eta\left(2\cos\frac{\pi p}{2} + \cos\pi p\right). \tag{8}$$

The DO_{22} structure is the equilibrium structure of Ni_3V and also of some ternary alloys based on Ni_3Mo where Mo is partially substituted by Al, Ti, Ta and Nb. In a stoichiometric ($x = 1/4$) and fully ordered alloy ($\eta = 1$) the (420) layering sequence is, 'Mo Ni Ni Ni Mo…'. It can be seen that apart from the four layer stacking of

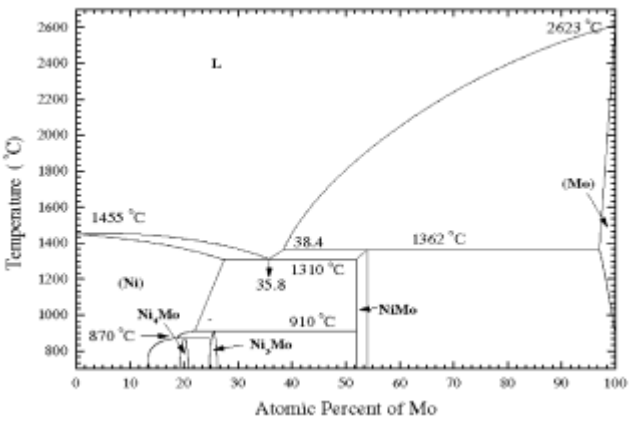

Figure 4. The NiMo phase diagram.

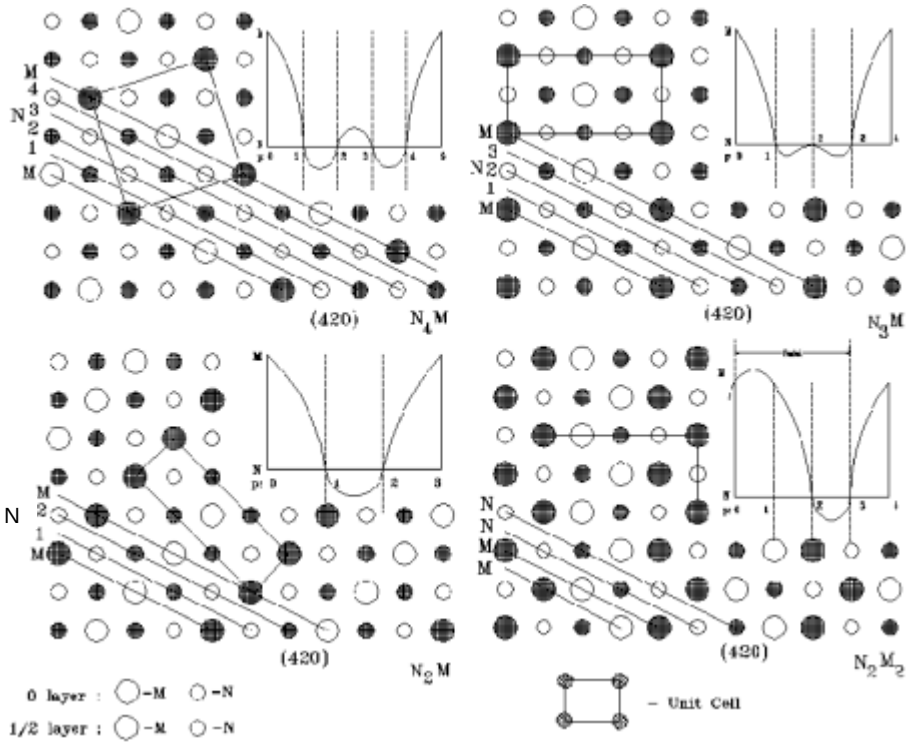

Figure 5. The description of four *fcc*-based superstructures in terms of stacking of (420) planes in the [001] projections and static concentration waves. The sequences of Ni (N) and Mo (M) of (420) planes and subunit cell clusters are also shown.

(420) planes, there exists a concentration modulation in the [010] direction in the DO_{22} structure. In fact, this structure can be viewed as a superposition of $\frac{i}{4}\langle 420\rangle$ $(i = 1, 3)$ and $\frac{2}{4}\langle 420\rangle \equiv \langle 100\rangle$ concentration waves.

Ni_2Mo (Pt_2Mo type) structure

The N_2M structure can be represented by a layered structure of (420) planes and the occupation probability of M atoms on the pth plane can be described by the concentration wave (figure 5)

$$C(p) = x + \frac{2}{3}\boldsymbol{h}\left(\cos\frac{2\boldsymbol{p}p}{3}\right). \tag{9}$$

The stoichiometric fully ordered alloy exhibits a layering sequence of (420) planes of 'Mo Ni Ni Mo…'. This structure can be viewed as a super-imposition of $\frac{i}{3}\langle 420\rangle$ $(i = 1, 2)$ waves.

Ni_2Mo_2 structure

This structure can be constructed from the concentration wave with the $\langle 1\frac{1}{2}0\rangle$ wave vector. The significance of this vector is that it terminates on a special point in the *fcc* reciprocal lattice where symmetry elements intersect. The concentration wave associated with this structure is given by

$$C(p) = x + \frac{\boldsymbol{h}}{\sqrt{2}}\sin\frac{\boldsymbol{p}}{2}\left(p + \frac{1}{2}\right). \tag{10}$$

For $x = 0{\cdot}5$ and $\boldsymbol{h} = 1$, the layering sequence of (420) planes is 'Ni Ni Mo Mo Ni Ni…'. This structure can be viewed as a super-imposition of $\frac{i}{4}\langle 420\rangle$ $(i = 1, 3)$ concentration waves.

1.3b *The free energy expressions for the superstructures:* The concentration wave free energy expressions for these *fcc*-based ordered super-lattice structures of the (420) family have been derived as follows:

N_4M ($D1_a$) structure

The sub-lattice occupation probabilities for the $D1_a$ structure are given as

$$\mathcal{N}_1 = x + 4Q(\underline{k}) \quad \text{and} \quad \mathcal{N}_2 = x - Q(\underline{k}),$$

giving rise to

$$\mathcal{N}_1 = x(1 + 4\tilde{\boldsymbol{h}}(\underline{k})) \quad \text{and} \quad \mathcal{N}_2 = x(1 - \tilde{\boldsymbol{h}}(\underline{k})).$$

The internal energy is given by

$$E^{D1_a} = \frac{1}{2}\left\{\left(V(000) + \left[\sum_{i=1}^{4} V\left(\frac{i}{5}\langle 420\rangle\right)\tilde{h}^2 \right] x^2 \right)\right\},$$

and the entropy is given by

$$S^{D1_a} = -\frac{k_B}{5}\{4\mathcal{F}(\mathcal{N}_2) + \mathcal{F}(\mathcal{N}_1)\},$$

with $\mathcal{F}(y) \equiv y\ln y + (1-y)\ln(1-y)$.

$N_3M(DO_{22})$ structure

Here, we have three sub-lattices with occupation probabilities given as

$$\mathcal{N}_1 = x(1+\tilde{h}^{(1)} + 2\tilde{h}^{(2)}), \quad \mathcal{N}_2 = x(1+\tilde{h}^{(1)} - 2\tilde{h}^{(2)})$$

$$\text{and} \quad \mathcal{N}_3 = x(1-\tilde{h}^{(1)}),$$

where $\tilde{h}^{(1)}$ and $\tilde{h}^{(2)}$ are the order parameters belonging to $\langle 1\frac{1}{2}0\rangle$ and $\langle 100\rangle$ wave vectors, respectively. The internal energy is given by

$$E^{DO_{22}} = \frac{1}{2}\left\{\left(V(000) + \left[V\left(\frac{1}{4}\langle 420\rangle\right)\tilde{h}^{(1)^2} + V\left(\frac{2}{4}\langle 420\rangle\right)\tilde{h}^{(2)^2} + V\left(\frac{3}{4}\langle 420\rangle\right)\tilde{h}^{(1)^2}\right]\right)x^2\right\},$$

and the entropy is given by

$$S^{DO_{22}} = -\frac{k_B}{4}\{\mathcal{F}(\mathcal{N}_1) + \mathcal{F}(\mathcal{N}_2) + 2\mathcal{F}(\mathcal{N}_3)\}.$$

N_2M (Pt_2Mo) structure

The sub-lattice occupation probabilities for the N_2M structure are given as

$$\mathcal{N}_1 = x(1+2\tilde{h}) \quad \text{and} \quad \mathcal{N}_2 = x(1-\tilde{h}).$$

The internal energy is given by

$$E^{N_2M} = \frac{1}{2}\left\{\left(V(100) + \left[\sum_{i=1}^{2} V\left(\frac{i}{3}\langle 420\rangle\right)\tilde{h}^2 \right]\right) x^2\right\},$$

and the entropy is given by

$$S^{N_2M} = -\frac{k_B}{3}\{2\mathcal{F}(\mathcal{N}_2) + \mathcal{F}(\mathcal{N}_1)\}.$$

$N_2M_2(I4_1/amd)$ structure

The sub-lattice occupation probabilities for the N_2M_2 structure are given as

$$\mathcal{N}_1 = x(1+\tilde{h}) \quad \text{and} \quad \mathcal{N}_2 = x(1-\tilde{h}).$$

The internal energy is given by

$$E^{N_2M_2} = \frac{1}{2}\left\{\left(V(000) + \left[V\left(\frac{1}{4}\langle 420\rangle\right) + V\left(\frac{3}{4}\langle 420\rangle\right)\right]\tilde{h}^2 \right) x^2\right\},$$

and the entropy is given by

$$S^{N_2M_2} = -\frac{k_B}{2}\{\mathcal{F}(\mathcal{N}_2) + \mathcal{F}(\mathcal{N}_1)\}.$$

1.3c *Ground state analysis:* At zero temperature, there is no contribution from entropy to the free energy of a solid solution and therefore its stability is governed by the internal energy alone, which is a function of effective pair interactions. In figure 6, we have given the values of these EPIs ($V_n(x)$, $n = 1, 4$) up to the fourth nearest neighbour pairs for *fcc*-based Ni–Mo alloys, calculated using the ASR–OP method.

The occurrence of ordering and clustering instabilities in solid solutions has been analysed by Clapp and Moss (1966) and de Fontaine (1975, 1981), whereas the interplay between the clustering and ordering instabilities have been examined by Kulkarni and Banerjee (1988) in terms of concentration waves with wave vector $\underline{k}$ which terminate at the so-called special points in the reciprocal lattice.

These special points are of interest as these are the locations of the extrema of the k-space potential energy function, $V(\underline{k})$, i.e. corresponding to $\partial V(\underline{k})/\partial \underline{k} = 0$. The nature of the extrema (minima/maxima/saddle point) is

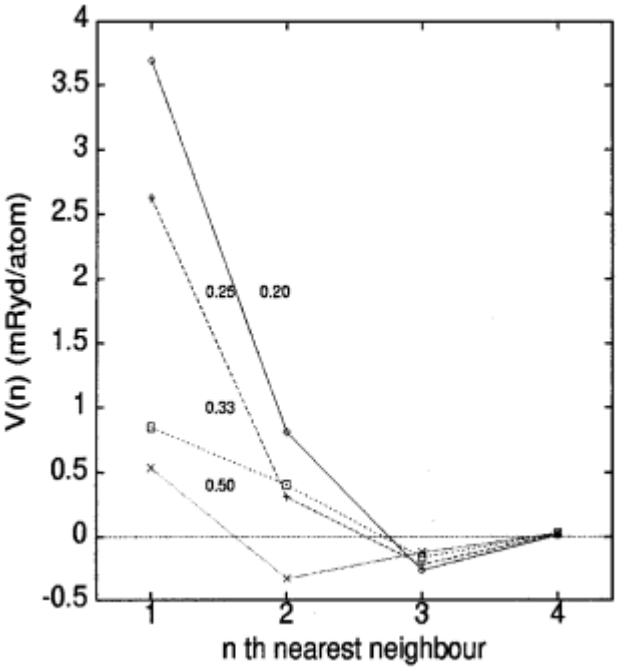

Figure 6. The variation of pair energies as a function of distance up to the sixth nearest neighbours for NiMo at different concentrations of Mo.

determined by the second derivative of the free energy function. Therefore, concentration waves with a wave vector, $\underline{k}$, which corresponds to a minimum of $V(\underline{k})$ are characterized by maximum value of instability temperature (T_i) and the amplification rate ($\alpha(\underline{k})$). A *fcc* solid solution may exhibit the following special point instabilities: (a) $\langle 000 \rangle$ or the clustering instability leading to spinodal phase separation and (b) $\langle 100 \rangle$, $\langle \frac{1}{2}\frac{1}{2}\frac{1}{2} \rangle$ and $\langle 1\frac{1}{2}0 \rangle$ ordering instabilities. The ordered structures generated by the amplification of a single variant of the $\langle \frac{1}{2}\frac{1}{2}\frac{1}{2} \rangle$ or the $\langle 1\frac{1}{2}0 \rangle$ waves obey the Landau–Lifshitz rules I, II and III (de Fontaine 1975, 1981) and are, therefore, candidates for the order–disorder transformation of the second kind. In the case of $\langle \frac{1}{2}\frac{1}{2}\frac{1}{2} \rangle$ and $\langle 1\frac{1}{2}0 \rangle$ ordering the coefficients of the third order term in the Landau–Lifshitz free energy expansion is equal to zero from symmetry considerations.

Kulkarni *et al* (1988) have analysed the $\langle 100 \rangle$, $\langle \frac{1}{2}\frac{1}{2}\frac{1}{2} \rangle$ and $\langle 1\frac{1}{2}0 \rangle$ special point ordering instabilities by considering (concentration-independent) effective pair interactions up to the third nearest neighbour pairs using the mean-field based SCW model. Their results for the $\langle 1\frac{1}{2}0 \rangle$ special point ordering instability in the V_2/V_1–V_3/V_1 space are shown in figure 7, where the horizontally-hatched portion represents the region of absolute minimum of $V\langle 1\frac{1}{2}0 \rangle$ in the EPI space. The region below the dashed line represents region of phase separation of ordered solid solution into a pure A and an ordered $A_{1-x}B_x$ phase and the vertically-hatched portion represents region of combined $\langle 1\frac{1}{2}0 \rangle$ ordering and subsequent phase separation. We have calculated these EPIs (concentration dependent) up to the fourth coordination shell for the *fcc* Ni–Mo alloys using the ASR–OP method. Our values of V_2/V_1 and V_3/V_1 at the four compositions viz. 20, 25, 33 and 50 at% of Mo have been superimposed on to figure 7. These ratios of our calculated EPIs have been observed to be in the region corresponding to the minimum of $V(1\frac{1}{2}0)$ i.e. $\langle 1\frac{1}{2}0 \rangle$ ordering instability exists in the Ni–Mo alloys.

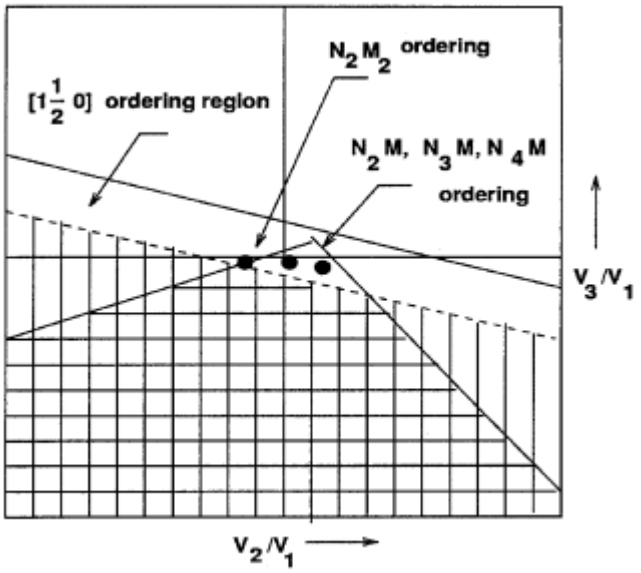

Figure 7. The $\langle 1\frac{1}{2}0 \rangle$ special point instability diagram, calculated using the CW model, marking different regions in the EPI-space where clustering and/or ordering instabilities exist. Superimposed on it are our ASR–OP calculated ratios of EPIs.

The ordering energies ($E_\Phi^{\text{ord}} = E_\Phi - E^{\text{dis}}$) of all the four ordered structures (Φ) which are members of (420) family, calculated using the SCW model (Khatchaturyan 1978, 1983), at different compositions are given in table 1. We will now examine the relative ground state phase stability of these ordered superstructures (Φ) from their ordering energy values, as calculated above, and compare our results with those observed experimentally. For Ni_3Mo based alloys, we immediately see that

$$E_{N_2M_2}^{\text{ord}} < E^{\text{dis}} \quad \text{at} \quad x_{\text{Mo}} = 0{\cdot}25, \tag{11}$$

indicating that N_2M_2 ordering instability exists in the disordered solid solution.

Since the introduction of a $\langle 100 \rangle$ concentration wave (secondary ordering) in a $\langle 1\frac{1}{2}0 \rangle$ ordered alloy of N_3M composition gives rise to DO_{22} structure, the DO_{22} structure should be more stable than the off-stoichiometric N_2M_2 structure. From table 1, we see that

$$E_{N_3M}^{\text{ord}} < E_{N_2M_2}^{\text{ord}} \quad \text{at} \quad x_{\text{Mo}} = 0{\cdot}25. \tag{12}$$

The secondary $\langle 1\frac{1}{2}0 \rangle$ ordering in a direction perpendicular to the original $\langle 1\frac{1}{2}0 \rangle$ vector gives rise to a structure which contains an ordered arrangement of N_4M and N_2M-subunit cell clusters. The condition for the stability of such a structure relative to the N_2M_2 structure can be seen to be satisfied from our ASR–OP calculations as

$$\frac{1}{2}[E_{N_4M}^{\text{ord}} + E_{N_2M}^{\text{ord}}] < E_{N_2M_2}^{\text{ord}} \quad \text{at} \quad x_{\text{Mo}} = 0 \cdot 25. \tag{13}$$

Table 1. The CW ordering energy ($E_\Phi^{\text{ord}} = E_\Phi - E^{\text{disordered}}$) values of all the ordered phases (Φ) of (420) family of Ni–Mo alloy system as a function of composition.

Phase (Φ)	Composition (at% Mo)	E_Φ^{ord} (K)
N_4M	0·20	−143·45
	0·25	−224·15
N_3M	0·20	−95·18
	0·25	−148·71
N_2M	0·20	−22·79
	0·25	−35·61
	0·33	−62·05
N_2M_2	0·20	−24·62
	0·25	−38·47
	0·50	−153·89

Hence, the super-imposition of (a) $\langle 100 \rangle$ and $\langle 1\tfrac{1}{2}0 \rangle$ concentration waves or (b) two mutually perpendicular $\langle 1\tfrac{1}{2}0 \rangle$ concentration waves always results in a structure of lower internal energy than the off-stoichiometric N_2M_2 structure. Further, we also see that

$$E^{\text{ord}}_{N_3M} < \frac{1}{2}[E^{\text{ord}}_{N_4M} + E^{\text{ord}}_{N_2M}] \quad \text{at} \quad x_{\text{Mo}} = 0{\cdot}25. \tag{14}$$

This prediction of stability of DO_{22} structure compared to the mixture of $D1_a$ and Pt_2Mo is contrary to experimental findings. We, however, notice that the difference between the formation energies of N_3M on one hand and a mixture of N_4M and N_2M on the other, is extremely small. Since these two alternatives are energetically comparable, the preference for one of them to form changes with minor variation in alloy composition. While in binary alloys close to $Ni_{75}Mo_{25}$ the $N_4M + N_2M$ develops during the early stage of ordering, the N_3M (DO_{22}) should become more favourable in several ternary alloys.

The ground state stability analysis at $x_{\text{Mo}} = 0{\cdot}20$ shows the hierarchy as

$$E^{\text{ord}}_{N_4M} < E^{\text{ord}}_{N_2M_2} < E^{\text{dis}},$$

which is consistent with the experimental findings.

1.3d *Finite temperature analysis:* We have calculated free energies of these superstructures, as functions of temperature, composition and order parameter using the static concentrations wave model (Khatchaturyan 1983) where we have taken the single-site approximation for the estimation of entropy. Under this approximation, the long-range correlations are properly treated but short-range correlations beyond a single site are ignored.

The instability temperature (T_{i}^{-}), defined as the temperature corresponding to the onset of ordering instability in the solid solution, is given in the SCW model by

$$T_{\text{i}}^{-} = -\frac{V(\underline{k})}{k_{\text{B}}} x(1-x), \tag{15}$$

for the ordering wave vector, $\underline{k}$.

The ordering free energy ($F^{\text{ord}} = F^{\Phi} - F^{\text{dis}}$) as a function of normalized order parameter $(\tilde{\eta})$ for the N_2M_2 phase at the stoichiometric compositions, $x_{\text{Mo}} = 0{\cdot}50$ and $x_{\text{Mo}} = 0{\cdot}20$, are plotted in figure 8. The temperature range has been chosen to be around the instability temperature ($T_{\text{i}} \equiv T_{\text{c}}$) at a given composition. These Landau plots, which we have generated from our first-principles calculations, show that the curvature of the F^{ord} vs $\tilde{\eta}$ changes the sign from positive to negative at T_{c}, as expected from a second order phase transition. The N_2M_2 instability temperatures for different alloy compositions, in the binary Ni–Mo system, essentially give the ordering spinodal line which was reported (schematically) earlier by de Fontaine (1975).

Figure 9 shows the variation of ordering free energy of $D1_{\text{a}}$ structured N_4M phase with the order parameter at the stoichiometric compositions $x_{\text{Mo}} = 0{\cdot}2$ and $x_{\text{Mo}} = 0{\cdot}25$. It may be noted that the plot (II) in figure 9(a) corresponds to the order–disorder transition temperature, T_{c}, at which the disordered state $(\tilde{\eta} = 0)$ and the ordered state $(\tilde{\eta} = \tilde{\eta}_{\text{c}})$ have the same free energy. The hump between these two states represents free energy barrier at T_{c},

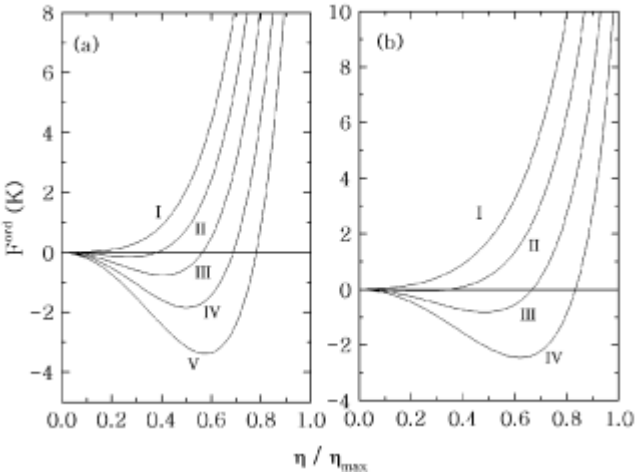

Figure 8. The ordering free energy of the N_2M_2 phase plotted as a function of $\tilde{\eta}$ at the stoichiometric composition, (**a**) $x_{\text{Mo}} = 0{\cdot}50$ and (**b**) $x_{\text{Mo}} = 0{\cdot}20$, respectively, at several temperatures around the instability temperature ($T_{\text{i}} \equiv T_{\text{c}}$). (a) Plots I–V correspond to $\frac{T}{T_{\text{c}}} = 1{\cdot}02$, 0·98, 0·95 and 0·92, respectively. (b) Plots I–IV correspond to $\frac{T}{T_{\text{c}}} = 1{\cdot}01$, 0·95, 0·88 and 0·83, respectively.

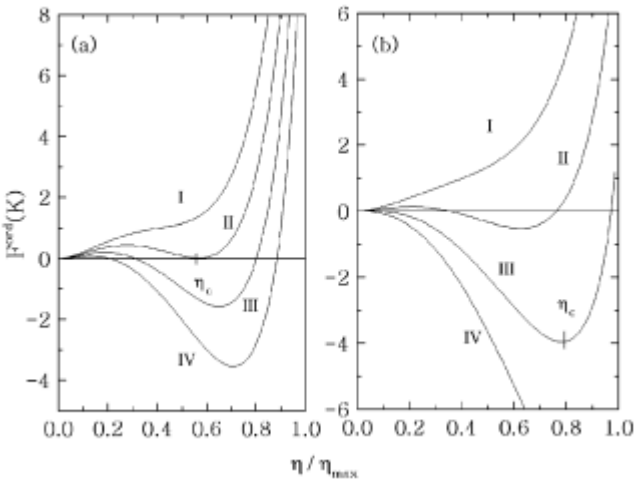

Figure 9. The variation of ordering free energy of N_4M phase with the order parameter at the stoichiometric composition: (**a**) $c_{\text{Mo}} = 0{\cdot}2$ and (**b**) $c_{\text{Mo}} = 0{\cdot}25$, respectively, at several temperatures around the transition temperature (T_{c}). (**a**) Plots I–IV correspond to $\frac{T}{T_{\text{c}}} = 1{\cdot}03$, 1·00, 0·97 and 0·94, respectively and (**b**) plots I–IV correspond to $\frac{T}{T_{\text{c}}} = 1{\cdot}04$, 0·97, 0·90 and 0·83, respectively.

which is characteristic of first order transitions. Figure 9(b) illustrates that at a certain degree of under-cooling, instability with respect to ordering develops, as reflected by the negative curvature of the F^{ord} vs $\tilde{h}$ plots at $\tilde{h} = 0$. The temperature at which such an instability develops is defined as the instability temperature (T_i) which can be determined from these plots for different super-lattice structures (both equilibrium and metastable) belonging to the (420) family.

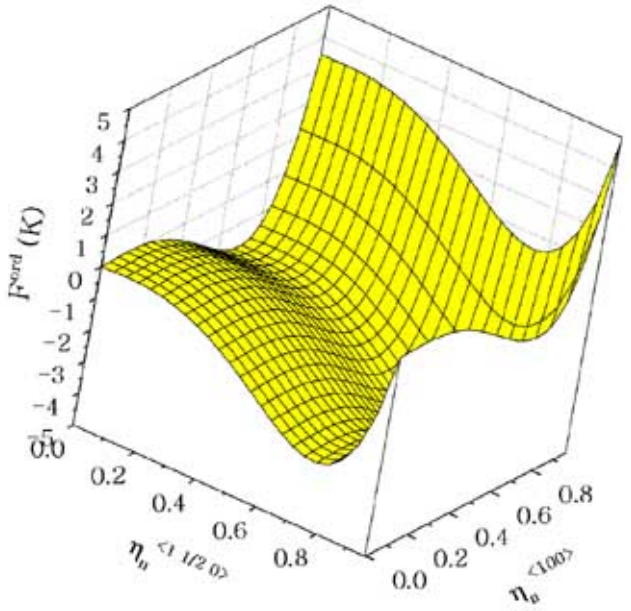

Figure 10. The variation of free energy of ordering of *DO* phase with the order parameters ($h_n^{\langle 1\frac{1}{2}0\rangle}$ and $h_n^{\langle 100\rangle}$) corresponding to $\langle 1\frac{1}{2}0\rangle$ and $\langle 100\rangle$ wave vectors at $\frac{T}{T_c} = 0{\cdot}92$.

The DO_{22}-structured N_3M phase, which closely competes with the HCP-based DO_a structure, has two order parameters ($h_n^{(1)}$ and $h_n^{(2)}$) belonging to $\langle 1\frac{1}{2}0\rangle$ and $\langle 100\rangle$ wave vectors, respectively. The free energies of ordering of the DO_{22} phase as a function of these two order parameters at the composition, $x_{Mo} = 0{\cdot}25$ are shown in figure 10. The stability domain of the DO_{22} phase corresponds to the region of negative free energy values.

Let us now consider a situation when a first order ordering process competes with a second order ordering. The completely disordered Ni_4Mo ($c_{Mo} = 0{\cdot}20$) alloy experiences both kinds of ordering tendencies viz. the second order $\langle 1\frac{1}{2}0\rangle$ ordering and the first order $\frac{1}{5}\langle 420\rangle$ ordering. For illustrative purpose, we have calculated the free energy of this alloy, F^{Ni_4Mo} ($h_n^{\langle 1\frac{1}{2}0\rangle}, h_n^{\frac{1}{5}\langle 420\rangle}$) at a given temperature as

$$F^{Ni_4Mo}\left(h_n^{\langle 1\frac{1}{2}0\rangle}, h_n^{\frac{1}{5}\langle 420\rangle}\right)$$

$$= \frac{1}{2}\left[F^{N_4M}\left(h_n^{\frac{1}{5}\langle 420\rangle}\right) + F^{N_2M_2}\left(h_n^{\langle 1\frac{1}{2}0\rangle}\right)\right],$$

at $x_{Mo} = 0{\cdot}20$.

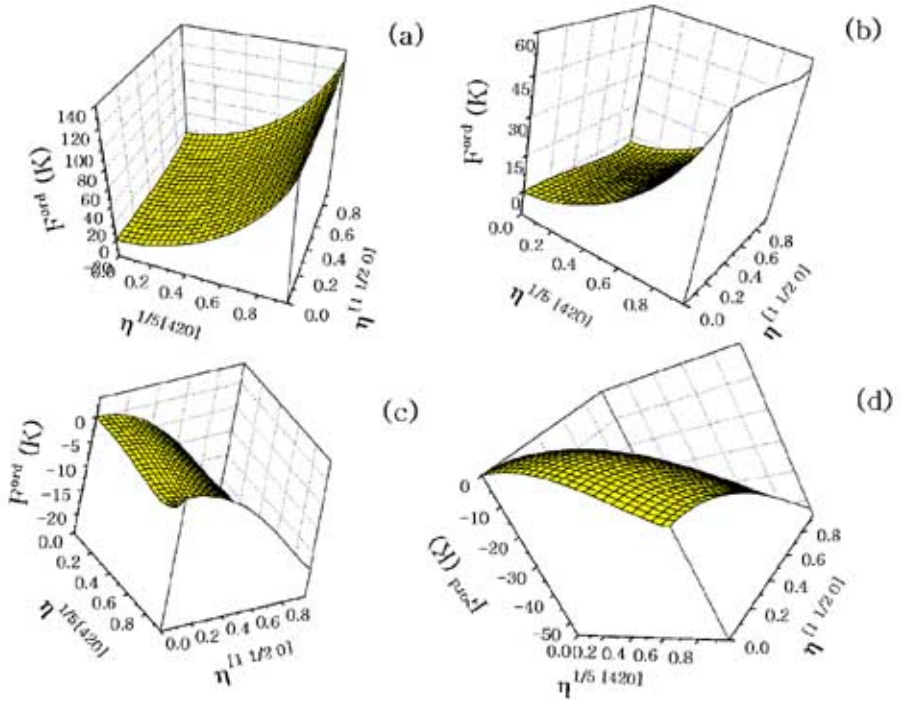

Figure 11. The ordering free energy of the Ni_4Mo-based alloy, exhibiting the $\langle 1\frac{1}{2}0\rangle$ and the $\frac{1}{5}(420)$ ordering tendencies, plotted as a function of order parameters for the corresponding ordering wave vector at four different temperatures. Figures (**a**) to (**d**) in the decreasing temperature sequence (see text for details).

The criterion of stability with respect to fluctuation in order parameter for a given wave vector can be determined by examining the curvature of the F vs $\tilde{\eta}$ plots at $\tilde{\eta} = 0$. Our results have been given in figure 11, for illustrating the following 4 distinct situations:

(a) Positive curvatures for both $\langle 1\frac{1}{2}0\rangle$ and $\frac{1}{5}\langle 420\rangle$, ordering, implying stability of the disordered state (figure 11(a)).

(b) Negative curvature for $\langle 1\frac{1}{2}0\rangle$ and positive curvature for $\frac{1}{5}\langle 420\rangle$, implying instability of the system for $\langle 1\frac{1}{2}0\rangle$ ordering, and no ordering tendency along $\frac{1}{5}\langle 420\rangle$ (figure 11(b)).

(c) Negative curvature for $\langle 1\frac{1}{2}0\rangle$, and positive for $\frac{1}{5}\langle 420\rangle$ at $\eta = 0$, but a dip in the free energy plot with respect to $\frac{1}{5}\langle 420\rangle$ near $\eta = 0{\cdot}8$. This implies that the system experiences simultaneous ordering tendencies towards $\langle 1\frac{1}{2}0\rangle$ ordering (second order) and $\frac{1}{5}\langle 420\rangle$ (first order) (figure 11(c)).

(d) Negative curvature along both $\langle 1\frac{1}{2}0\rangle$ and $\frac{1}{5}\langle 420\rangle$, i.e. system experiences instabilities for $\langle 1\frac{1}{2}0\rangle$ and $\frac{1}{5}\langle 420\rangle$ ordering simultaneously (figure 11(d)).

Although $D1_a$ is the stable equilibrium structure at $x_{\mathrm{Mo}} = 0{\cdot}20$, a stronger tendency for the development of $\langle 1\frac{1}{2}0\rangle$ ordering can be noticed in the initial stages of ordering, as reflected by a larger negative curvature of the free energy surface at $\eta_n^{\langle 1\frac{1}{2}0\rangle} = \eta_n^{\frac{1}{5}\langle 420\rangle} = 0$ along the $\eta_n^{\langle 1\frac{1}{2}0\rangle}$ axis compared to that of $\eta_n^{\frac{1}{5}\langle 420\rangle}$ axis (figure 11(a)). The curvature of the free energy surface is negative in both the directions in figure 11(d) which suggests that homogeneous ordering is possible for both the ordering processes. A mixed state consisting of concentration waves with wave vector ranging from $\langle 1\frac{1}{2}0\rangle$ to $\frac{1}{5}\langle 420\rangle$ is encountered on the path of the ordering process at sufficiently low temperatures (Banerjee *et al* 1984).

References

Andersen O K 1975 *Phys. Rev.* **B12** 3060

Andersen O K and Jepsen O 1984 *Phys. Rev. Lett.* **53** 2571

Andersen O K, Jepsen O and Krier H 1991 *Electronic structure of metals and alloys* (eds) O K Andersen *et al* (Singapore: World Scientific)

Arya A, Banerjee S, Das G P, Dasgupta I, Saha-Dasgupta T and Mookerjee A 2001 *Acta Mater.* **49** 3575

Banerjee S, Urban K and Wilkens M 1984 *Acta Metall.* **32** 299

Burke N R 1976 *Surf. Sci.* **58** 349

Clapp P C and Moss S C 1966 *Phys. Rev.* **142** 418

Dasgupta I, Saha T and Mookerjee A 1995 *Phys. Rev.* **B51** 3413

de Fontaine D 1975 *Acta Metall.* **23** 553

de Fontaine D in *Solid-state phase transformations* (eds) H I Aaronson *et al* (USA: Metall. Soc. AIME) p. 25

Kaplan T and Gray L J 1976 *Phys. Rev.* **B14** 3462

Kaplan T and Gray L J 1977 *Phys. Rev.* **B15** 3260

Kaplan T and Gray L J 1978 *Phys. Rev.* **B12** 4607

Kaplan T, Gray L J, Leath P L and Diehl H W 1980 *Phys. Rev.* **B21** 4230

Khatchaturyan A G 1978 *Prog. Mater. Sci.* **22** 1

Khatchaturyan A G 1983 *Theory of structural transformations in solids* (New York: Wiley)

Kulkarni U D and Banerjee S 1988 *Acta Metall.* **36** 413

Kumar V, Mookerjee A and Srivastava V K 1982 *J. Phys. C: Solid State Phys.* **15** 1939

Mookerjee A 1973 *J. Phys. C: Solid State Phys.* **6** L205, 1340

Saha T and Mookerjee A 1997 *J. Phys.: Condens. Matter* **10** 2179

Saha T, Dasgupta I and Mookerjee A 1994 *J. Phys.: Condens. Matter* **6** L245

Shield J E and Williams R K 1987 *Scr. Metall.* **21** 1475

Shunk F A 1969 in *Constitution of binary alloys* (New York: McGraw-Hill) 2nd Suppl.

Wang Y, Faulkner J S and Stocks G M 1993 *Phys. Rev. Lett.* **70** 3287

Wolverston C, Ceder G, de Fontaine D and Dreyssé H 1993 *Phys. Rev.* **B48** 5766